NBO analysis and UV-Visible analysis of Anions of Enol form of Isatin and its Halogenated Derivatives: A Theoretical Study

Esha Arora[1*] and Sunita Gulia[2]
[1]*Department of Chemistry, Shyama Prasad Vidyalaya Lodi Estate, New Delhi-110003*
[2]*Department of ICT & Training, Central Institute of Educational Technology, National Council of Educational Research and Training, Sri Aurobindo Marg, New Delhi-110016*

Abstract- This work presents a comprehensive theoretical investigation of the anionic enol form of isatin and its halogenated derivatives, integrating Natural Bond Orbital (NBO) analysis with Time-Dependent Density Functional Theory (TD-DFT) based UV-Visible spectroscopic studies. Although isatin derivatives have been widely explored for their chemical and biological relevance, the electronic structure of their anionic enol forms**, particularly under the influence of halogen substitution, remains largely unexamined. This study fills that gap by offering the** first systematic correlation **between** donor–acceptor interactions **obtained from NBO analysis and the** electronic excitation patterns **observed in UV-Visible spectra. NBO analysis reveals pronounced π-delocalization and significant lone-pair to antibonding interactions, which become further amplified upon halogen substitution. These electronic effects directly influence the nature of the low-lying excited states, as reflected in the TD-DFT predicted absorption bands. A clear structural–spectral relationship emerges, demonstrating how halogens alter electron density distribution, stabilize specific resonance forms, and modulate the intensity and position of key electronic transitions. The novelty of the present work lies in establishing a direct and unified theoretical framework that links intramolecular charge transfer pathways with spectroscopic response behavior in isatin-based anions. This integrated approach provides new insights into substituent-controlled electronic tuning and offers valuable guidance for the rational design of functional isatin derivatives in optoelectronic, photochemical, and pharmaceutical applications.**

Keywords: Anion, DFT, Donor–Acceptor Interaction, Enol Form, Halogenated Derivatives, Isatin, NBO Analysis, TD-DFT, UV-Visible Spectroscopy.

I. INTRODUCTION

Isatin (1H-indole-2,3-dione) and its substituted derivatives constitute an important class of heterocyclic compounds due to their versatile chemical reactivity and wide-ranging applications in medicinal chemistry, materials science, and biological systems [1–3]. The presence of adjacent carbonyl groups within the indole framework makes isatin particularly interesting from both structural and electronic perspectives, as it can exist in multiple tautomeric forms, primarily the keto and enol forms. Among these, the enol form gains special significance under deprotonated or anionic conditions, where enhanced electron delocalization substantially influences molecular stability, reactivity, and spectroscopic behavior [4].

Halogen substitution on the isatin scaffold further modifies its electronic structure through inductive and mesomeric effects, thereby affecting intramolecular charge transfer, orbital overlap, and hydrogen-bonding characteristics [5,6]. Such substitutions are known to fine-tune physicochemical properties, making halogenated isatin derivatives valuable candidates for theoretical and spectroscopic investigations. Although numerous experimental and computational studies have focused on neutral isatin derivatives, detailed insight into the anionic enol forms, particularly with respect to orbital interactions and spectral signatures, remains limited.

Natural Bond Orbital (NBO) analysis has proven to be a powerful theoretical approach for understanding bonding characteristics, hyperconjugative interactions, charge delocalization, and stabilization energies in molecular systems [7,8]. By quantitatively

describing donor–acceptor interactions, NBO analysis offers a deeper understanding of electronic structure beyond conventional molecular orbital interpretations. This approach becomes especially relevant for anionic species, where redistribution of electron density plays a decisive role in molecular stabilization. UV–Vis spectroscopy is particularly useful for analyzing electronic transitions and intramolecular charge-transfer effects [9].

In our earlier theoretical investigation, a comprehensive study was carried out on the neutral forms of isatin and its halogenated derivatives, emphasizing structural, electronic, and spectroscopic properties [10]. Additionally, related computational and spectroscopic aspects of isatin derivatives have been explored in our previous work published in the *Journal of Emerging Technologies and Innovative Research*, further establishing the relevance of density functional theory in understanding structure–property relationships in such heterocyclic systems [11].

The present study is a direct continuation of these investigations, extending the analysis to the anions of the enol forms of isatin and its halogenated derivatives. Density functional theory (DFT) calculations have been employed to perform detailed NBO analysis alongside simulated UV–Visible spectroscopic studies. This combined approach aims to elucidate the effects of deprotonation and halogen substitution on electronic structure, intramolecular interactions, and spectral characteristics. The results are expected to provide valuable theoretical insights that complement experimental findings and contribute to the rational design of isatin-based functional molecules.

II. COMPUTATIONAL DETAILS

All quantum chemical calculations in the present study were carried out using Density Functional Theory (DFT) as implemented in the Gaussian 09 program package [12]. Geometry optimizations of the anionic enol forms of isatin and its halogen-substituted derivatives were performed without imposing any symmetry constraints using the B3LYP hybrid exchange–correlation functional, which has been widely employed for reliable prediction of structural, electronic, and spectroscopic properties of heterocyclic systems [13–15]. The 6-311++G(d,p) basis set was used for all atoms to adequately account for polarization and diffuse functions, which are essential for a proper description of anionic species. All optimized geometries were confirmed as true minima on the potential energy surface by the absence of imaginary frequencies in the vibrational frequency calculations. Natural Bond Orbital (NBO) analysis was performed using the NBO 3.1 program integrated within Gaussian 09 to gain insight into bonding characteristics, charge distribution, hyperconjugative interactions, and stabilization energies [7,8]. Second-order perturbation theory analysis was employed to quantify donor–acceptor interactions, particularly lone-pair to antibonding orbital interactions, which play a significant role in stabilizing the anionic enol structures. The electronic absorption (UV–Vis) spectra were simulated using time-dependent density functional theory (TD-DFT) calculations at the same level of theory based on the optimized ground-state geometries. Vertical excitation energies, oscillator strengths, and the nature of electronic transitions were analyzed to interpret charge-transfer effects and the influence of halogen substitution in the anionic systems [16]. All calculations were performed in the gas phase to maintain consistency with earlier theoretical investigations, including our previous work [10,11] and related studies reported in the literature. The adopted computational protocol ensures a consistent and systematic evaluation of structural, electronic, NBO, and spectroscopic properties of isatin-based anionic systems.

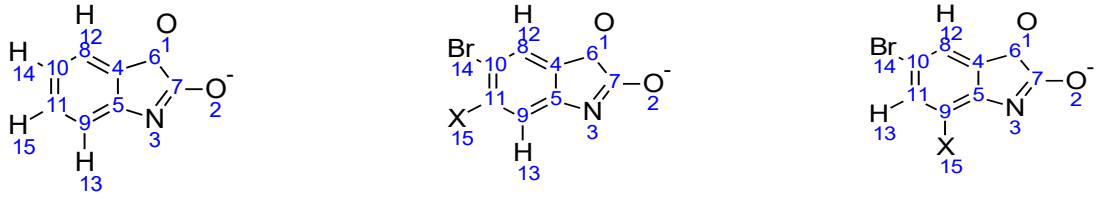

1a 1b 1c

Figure 1 Numbering scheme of enol form of anions of Isatin (1a), 10-Bromo-11-haloisatin (1b), 10-Bromo-9-haloisatin (1c)

III. RESULTS AND DISCUSSION

3.1 NBO Analysis

3.1.1 Donor–Acceptor Interactions

The Natural Bond Orbital (NBO) analysis reveals several highly stabilizing donor–acceptor interactions that contribute significantly to the electronic delocalization and resonance stabilization of the anionic enol form of isatin. The most prominent interaction observed in Table 1 is between the antibonding π-orbitals: $\pi^*(C8–C10) \rightarrow \pi^*$ (C4–C5), with an exceptionally high stabilization energy of 265.47 kcal/mol, indicating a strong conjugative resonance effect along the extended π-system. Other notable interactions include $n_2(N3) \rightarrow \pi^*(O2–C7)$ with 87.38 kcal/mol, $\pi^*(O1–C6) \rightarrow \pi^*$(O2–C7) at 86.90 kcal/mol, and $n_2(N3) \rightarrow \pi^*(C4–C5)$ showing 80.67 kcal/mol of stabilization. These n → π* and π → π* interactions strongly suggest intense electron delocalization within the molecular framework, facilitated by lone pairs on nitrogen and oxygen atoms engaging in conjugation with adjacent π* orbitals. Furthermore, interactions such as $n_2(O2) \rightarrow \sigma^*(C6–C7)$ indicate hyperconjugative stabilization, where lone pairs donate electron density into adjacent σ* orbitals, weakening σ-bonds slightly while enhancing overall molecular stability. The presence of σ → σ* interactions (e.g., $\sigma(N3–C5) \rightarrow \sigma^*$(O2–C7) suggests minor covalent bond weakening, characteristic of intramolecular hyperconjugation. Collectively, these interactions underscore a high degree of π-conjugation and resonance stabilization across the molecular scaffold. Lone pair delocalization from oxygen and nitrogen plays a pivotal role in stabilizing the anionic species. The magnitude of interaction energies confirms strong electronic stabilization, which has direct implications for the reactivity, structural rigidity, and spectroscopic features of the molecule.

S.No.	DONOR ORBITAL	OCCUPANCY	ENERGY	ACCEPTOR ORBITAL	OCCUPANCY	ENERGY	INTERACTON ENERGY (Kcal/mol)
1	π(O2-C7)	1.96739	-0.20402	n2(N3)	1.40369	-0.01544	7.23
2	π(O2-C7)	1.96739	-0.20402	π*(O1-C6)	0.14488	0.15838	4.73
3	σ(N3-C5)	1.97881	-0.63114	σ*(O2-C7)	0.01680	0.77117	5.6
4	σ(N3-C7)	1.98419	-0.62829	σ*(C5-C9)	0.02630	0.69661	5.88
5	π(C4-C5)	1.53229	-0.10285	N3 (n2)	1.40369	-0.01544	44.33
6	π(C4-C5)	1.53229	-0.10285	π*(O1-C6)	0.14488	0.15838	28.83
7	π(C4-C5)	1.53229	-0.10285	π*(C8-C10)	0.37828	0.14985	30.74
8	π(C4-C5)	1.53229	-0.10285	π*(C9-C11)	0.33152	0.15371	14.16
9	σ(C6-C7)	1.97669	-0.43478	σ*(C4-C8)	0.02552	0.72485	5.43
10	π(C8-C10)	1.70557	-0.12764	π*(C4-C5)	0.47824	0.16353	13.44
11	π(C8-C10)	1.70557	-0.12764	π*(C9-C11)	0.33152	0.15371	23.77
12	σ(C8-H12)	1.98007	-0.39579	σ*(C4-C5)	0.04217	0.67482	4.69
13	π(C9-C11)	1.73322	-0.12939	π*(C4-C5)	0.47824	0.16353	20.39
14	π(C9-C11)	1.73322	-0.12939	π*(C8-C10)	0.37828	0.14985	13.72
15	CR1(O1)	1.99975	-18.72025	RY*1(C6)	0.01667	0.98989	6.38
16	CR1(O2)	1.99975	-18.67718	RY*1(C7)	0.01562	1.02865	6.12
17	n1(O1)	1.98073	-0.55603	RY*1(C6)	0.01667	0.98989	16.60
18	n2(O1)	1.87973	-0.13101	σ*(C4-C6)	0.06337	0.61649	17.91
19	n2(O1)	1.87973	-0.13101	σ*(C6-C7)	0.15408	0.46057	23.80
20	n1(O2)	1.97974	-0.52483	RY*1(C7)	0.01562	1.02865	16.63
21	n2(O2)	1.87097	-0.09043	σ*(N3-C7)	0.05498	0.67492	19.56
22	n2(O2)	1.87097	-0.09043	σ*(C6-C7)	0.15408	0.46057	24.51
23	n1(N3)	1.92767	-0.20203	σ*(C4-C5)	0.04217	0.67482	7.68
24	n1(N3)	1.92767	-0.20203	σ*(C6-C7)	0.15408	0.46057	7.76
25	n2(N3)	1.40369	-0.01544	π*(O2-C7)	0.32426	0.17478	87.38
26	n2(N3)	1.40369	-0.01544	π*(C4-C5)	0.47824	0.16353	80.67
27	π*(O1-C6)	0.14488	0.15838	π*(O2-C7)	0.32426	0.17478	86.90
28	π*(C8-C10)	0.37828	0.14985	π*(C4-C5)	0.47824	0.16353	265.47

Table 1 NBO analysis of anion of enol form of ISTA

3.1.2 Graphical Representation of Donor–Acceptor Interactions

A graphical illustration of the donor–acceptor interactions identified through NBO analysis is presented in Figure 2. In this diagram, nodes represent molecular orbitals (either donor or acceptor), while arrows indicate the direction of electron donation. The edge labels display the second-order perturbation interaction energies (in kcal/mol), quantifying the extent of stabilization arising from each interaction. Key interactions include: *π(C8–C10) → π*(C4–C5)* with a high stabilization energy of 265.47 kcal/mol, indicating extensive π-conjugation and resonance, *n_2(N3) → π*(O2–C7)* (87.38 kcal/mol) and *π(O1–C6) → π*(O2–C7)* (86.90 kcal/mol), both contributing significantly to intramolecular charge transfer and resonance stabilization.

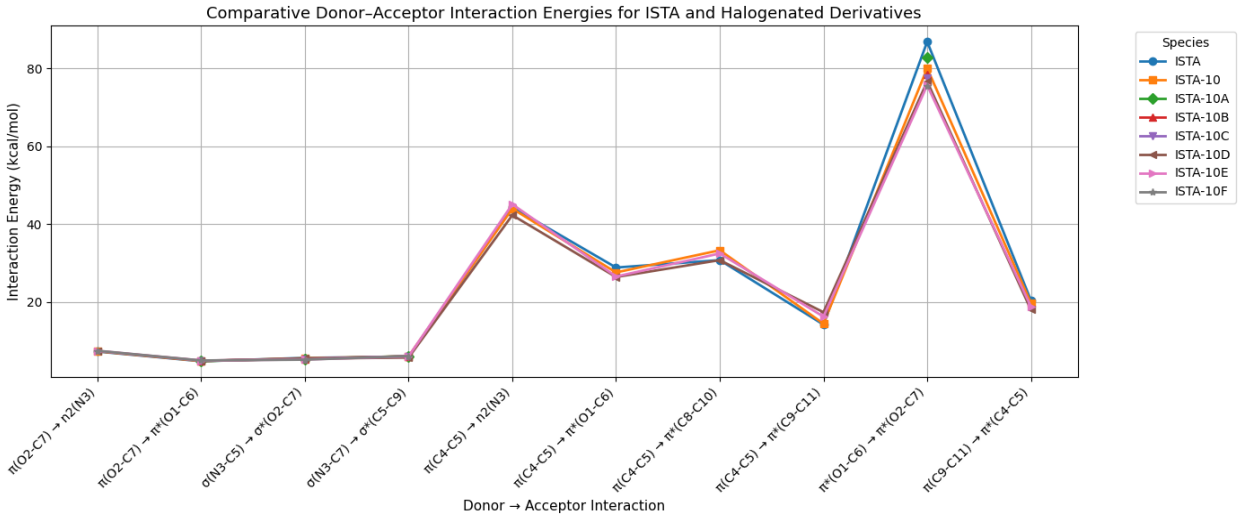

Figure 2 A graphical representation of the donor–acceptor interactions of ISTA and its halogenated derivatives identified through NBO analysis

Weaker yet relevant interactions such as *n_2(O2) → σ*(C6–C7)* and *σ(N3–C5) → σ*(O2–C7)* point to hyperconjugative effects that modulate covalent bond strengths and further stabilize the anionic structure. This visual representation provides a concise overview of the electronic delocalization pathways within the molecule. The NBO framework thus not only quantifies energetic contributions but also clarifies the topology of electron flow, revealing the molecular regions most involved in resonance and conjugation.

3.1.3 Effect of Halogen Substitution on Intramolecular Interactions

The introduction of halogen substituents (e.g., Br, Cl, F, I) into the lactim form of the anionic isatin derivatives has a pronounced impact on electron density distribution, resonance delocalization, and intramolecular donor–acceptor interactions. These effects arise due to the strong electron-withdrawing nature of halogens, which exert both inductive (-I) and resonance (-R or +R) influences on the molecular π-system. The interaction energy values presented in Table 2 provide a detailed picture of these changes. The observed π → π* and n → π* interactions reflect enhanced resonance stabilization and delocalization of electron density, particularly across the conjugated π-network of the isatin ring. These interactions suggest the persistence of aromatic or extended conjugative character even in the anionic forms, and their energy magnitudes vary systematically with the nature of the halogen atom. In addition, σ → σ* and n → σ* interactions, particularly involving C–X (X = halogen) bonds, indicate hyperconjugative effects and intramolecular electron density shifts driven by halogen substitution. For example, fluorine—with its strong electronegativity and lone pairs—often engages in n(F) → σ* interactions, whereas iodine—with larger polarizability—contributes to diffuse π-conjugation effects. These interactions influence both the electronic structure and stability of the molecule and are consistent with trends observed in the calculated UV–Visible spectra (discussed in later sections).

S.No.	DONOR ORBITAL	ACCEPTOR ORBITAL	ISTA	ISTA-10	ISTA-10A	ISTA-10B	ISTA-10C	ISTA-10D	ISTA-10E	ISTA-10F
1	π(O2-C7)	n2(N3)	7.23	7.3	-	-		7.34	7.41	7.43
2	π(O2-C7)	π*(O1-C6)	4.73	4.78	4.77	4.82	4.83	4.87	4.92	4.93
3	π(O1-C6)	π*(C4-C8)	-	-	4.53	4.58	4.59	-	-	-
4	π (N3-C5)	π*(O2-C7)	-	-	45.85	46	45.95	-	-	-
5	π (N3-C5)	π*(N3-C5)	-	-	5.5	5.46	5.44	-	-	-
6	π (N3-C5)	π*(C4-C8)	-	-	8.91	9.14	9.19	-	-	-
7	π (N3-C5)	π*(C9-C11)	-	-	8.5	9.35	9.42	-	-	-
8	σ(N3-C5)	σ*(O2-C7)	5.6	5.51	5.38	5.38	5.38	5.41	5.19	5.14
9	σ(N3-C7)	σ*(C5-C9)	5.88	5.99	6.04	6.00	6.01	5.67	5.97	6.06
10	σ(C4-C5)	σ*(C9-X15/H13)	-	-	-	-	-	5.00	6.23	7.01
11	σ(C6-C7)	σ*(C4-C8)	5.43	5.32	5.32	-	-	5.18		5.13
12	π(C4-C5)	n2(N3)	44.33	43.96	-	-	-	42.3	45.1	-
13	π(C4-C5)	π*(O1-C6)	28.83	27.57	-	-	-	26.39	26.52	-
14	π(C4-C5)	π*(C8-C10)	30.74	33.28	-	-	-	30.74	32.45	-
15	π(C4-C5)	π*(C9-C11)	14.16	14.4	-	-	-	17.34	16.21	-
16	π(C4-C8)	n1(C10)	-	-	46.18	46.7	-	-	-	-
17	π(C4-C8)	π*(O1-C6)	-	-	21.01	20.28	-	-	-	19.8
18	π(C4-C8)	π*(N3-C5)	-	-	25.23	25.2	-	-	-	
19	π(C4-C8)	π*(C5-C9)	-	-	-	-	-	-	-	20.29
20	π(C4-C8)	π*(C10-C11)	-	-	-	-	-	-	-	15.71
21	π(C5-C9)	n2(N3)	-	-	-	-	-	-	-	30.62
22	π(C5-C9)	π*(C4-C8)	-	-	-	-	-	-	-	13.61
23	π(C5-C9)	π*(C10-C11)	-	-	-	-	-	-	-	32.27
24	σ(C5-C9)	σ*(C11-X15)	-	-	4.11	4.88	5.4	-	-	-
25	σ(C8-C10)	σ*(C11-X15)	-	-	3.78	5.04	5.63	-	-	-
26	σ(C4-C8)	σ*(C10-Br14/H14)	-	6.37	5.9	5.52	5.4	6.52	6.39	6.33
27	σ(C6-C7)	σ*(C4-C8)	5.43	5.32	5.32	5.32	5.32	-	5.15	-
28	π(C8-C10)	π*(C4-C5)	13.44	12.02	-	-	-	12.85	12.73	-
29	π(C8-C10)	π*(C9-C11)	23.77	22.53	-	-	-	21.23	24.25	-
30	σ(C9-C11)	σ*(C10-C11)	2.79	-	5.57	4.92	-	-	-	-
31	σ(C9-C11)	σ*(C10-Br14/H14)	-	5.52	4.79	5.15	5.18	5.32	4.95	4.88
32	π(C9-C11)	n1(C10)	-	-	37.09	36.82	37.03	-	-	-
33	π(C9-C11)	π*(N3-C5)	-	-	25.7	23.36	22.9	-	-	-
34	π(C4-C8)	n1(C10)	-	-	46.18	-	46.6	-	-	-
35	π(C4-C8)	π*(O1-C6)	-	-	21.01	-	20.09	-	-	-
36	π(C4-C8)	π*(N3-C5)	-	-	25.23	-	25.17	-	-	-
37	σ(C8-H12)	σ*(C4-C5)	4.69	4.44	4.54	4.52	4.52	4.58	4.66	4.7

38	σ(C9-X15/H13)	σ*(C10-C11)	-	-	4.13	4.56	4.59	-	-	-
39	σ(C10-C11)	σ*(C9-X15/H13)	-	-	-	-	-	-	-	4.7
40	π(C10-C11)	π*(C4-C8)	-	-	-	-	-	-	-	21.9
41	π(C10-C11)	π*(C5-C9)	-	-	-	-	-	-	-	11.34
42	π(C9-C11)	π*(C4-C5)	20.39	19.72	-	-	-	17.97	18.82	-
43	π(C9-C11)	π*(C8-C10)	13.72	14.28	-	-	-	14.6	13.01	-
44	CR1(O1)	RY*1(C6)	6.38	6.42	6.42	6.42	6.42	6.45	6.44	6.44
45	CR1(O2)	RY*1(C7)	6.12	6.2	6.27	6.25	6.25	6.18	6.19	6.22
46	n1(O1)	RY*1(C6)	16.6	16.64	16.6	16.59	16.59	16.72	16.65	16.65
47	n2(O1)	σ*(C4-C6)	17.91	18.34	18.38	18.55	18.61	18.58	18.69	18.74
48	n2(O1)	σ*(C6-C7)	23.8	24.04	24.18	24.11	24.1	24.04	24.05	24.07
49	n1(O2)	RY*1(C7)	16.63	16.74	16.85	16.81	16.81	16.58	16.58	16.62
50	n2(O2)	σ*(N3-C7)	19.56	19.74	20.06	20.06	20.07	19.98	20.14	20.2
51	n2(O2)	σ*(C6-C7)	24.51	24.96	24.97	25.04	25.07	25.08	25.08	25.09
52	n1(N3)	RY*1(C5)	4.44	4.54	4.96	4.79	4.75	-	-	-
53	n1(N3)	σ*(C4-C5)	7.68	7.85	8.05	8.06	8.06	7.85	8.07	8.15
54	n1(N3)	σ*(C6-C7)	7.76	7.79	7.64	7.67	7.68	7.77	7.77	7.76
55	n2(N3)	π*(O2-C7)	87.38	85.3	-	-	-	83.93	82.7	82.34
56	n2(N3)	π*(C4-C5)	80.67	82.71	-	-	-	85.53	87.89	-
57	n2(N3)	π*(C5-C9)	-	-	-	-	-	-	-	98.28
58	n1(C10)	π*(C4-C8)	-	-	63.89	62.31	61.73	-	-	-
59	n1(C10)	π*(C9-C11)	-	-	70.1	68.13	67.28	-	-	-
60	n3(Br14)	n1(C10)	-	-	14.78	15.19	15.28	-	-	-
61	n1(X15)	RY*1(C11)	-	-	7.99	-	-	-	-	-
62	n1(X15)	RY*1(C9)	-	-	-	-	-	6.88	-	-
63	n2(X15)	σ*(C9-C11)	-	-	5.4	-	-	5.62	-	-
64	n2(X15)	σ*(C10-C11)	-	-	5.49	-	-	-	-	-
65	n2(X15)	σ*(C5-C9)	-	-	-	-	-	5.94	-	-
66	n3(X15)	π*(C9-C11)	-	-	18.07	-	9.07	16.66	11.04	-
67	n3(X15)	π*(C5-C9)	-	-	-	-	-	-	-	7.25
68	n3(Br14)	π*(C10-C11)	-	-	-	-	-	-	-	7.17
69	n3(Br14)	π*(C8-C10)	-	6.93	-	11.86	-	7.26	7.12	-
70	π*(O1-C6)	π*(O2-C7)	86.9	80.08	82.88	78.55	77.49	76.68	75.7	75.43
71	π*(C8-C10)	π*(C4-C5)	265.47	167.58	-	-	-	221.51	213.14	-
72	π*(C8-C10)	π*(C9-C11)	-	221.32	-	-	-	-	-	-
73	π*(C9-C11)	π*(C4-C5)	-	298.78	-	-	-	240.88	159.34	-
74	π*(N3-C5)	π*(O2-C7)	-	-	67.69	68.38	68.39	-	-	-
75	π*(N3-C5)	π*(C4-C8)	-	-	374.99	349.11	348.58	-	-	-
76	π*(C9-C11)	π*(C4-C8)	-	-	4.82	-	-	-	-	-
77	π*(C9-C11)	π*(N3-C5)	-	-	-	335.93	357.38	-	-	-

78	π*(C5-C9)	π*(C4-C8)	-	-	-	-	-	-	-	291.66
79	π*(C10-C11)	π*(C4-C8)	-	-	-	-	-	-	-	109.99
80	π*(C10-C11)	π*(C5-C9)	-	-	-	-	-	-	-	-

Table 2 NBO analysis of Comparison of Anions of Enol form of Halogenated Derivatives of Isatin

Overall, the NBO-derived interaction patterns reveal that halogen substitution modulates both the strength and nature of donor–acceptor interactions, thereby altering resonance pathways, electron delocalization, and the reactivity profile of these anionic systems.

3.1.4 Donor–Acceptor Interactions in Halogenated Isatin Anions

3.1.4.1 π → π Interactions and Ring Delocalization

The *π(C4–C5) → π*(C8–C10)* interaction (Row 14) exhibits a slight increase from 30.74 kcal/mol in ISTA to 33.28 kcal/mol in ISTA-10, indicating enhanced π-delocalization due to halogen substitution. More notably, the *π(N3–C5) → π*(O2–C7)* interaction (Row 4) appears only in dihalogenated derivatives (ISTA-10A, 10B, 10C), with stabilization energies around 45–46 kcal/mol, reflecting strong resonance enhancement caused by dual halogen substitution. One of the most striking findings is the exceptionally high energy of the *π*(N3–C5) → π**(C4–C8) interaction (Row 75), ranging from 374.99 to 348.58 kcal/mol, indicating extensive delocalization across the aromatic ring and suggesting robust resonance stabilization in these anionic systems. The gradual decrease in this interaction from bromo–fluoro to dibromo derivatives suggests that the strength of resonance correlates with the electron-withdrawing ability of the halogens at the C11 position. Similarly, the *π*(C9–C11) → π**(N3–C5) interaction (Row 77) shows high stabilization energies of 335.93 to 357.38 kcal/mol, peaking in ISTA-10C, confirming that this derivative has the strongest π-delocalization among the series. The *π*(O1–C6) → π**(O2–C7) interaction (Row 70), ranging from 75.43 to 86.90 kcal/mol, demonstrates consistent resonance stabilization within the carbonyl–enolate core, strongly influenced by halogenation. Meanwhile, the *π*(C8–C10) → π**(C4–C5) interaction (Row 71) shows a decline from 265 kcal/mol in ISTA to 167 kcal/mol in ISTA-10, indicating that halogenation may disrupt extended conjugation in some derivatives. Despite this, high-energy transitions like *π*(C9–C11) → π**(C4–C5) (Row 73, ~298.78 kcal/mol) confirm continued halogen-induced resonance stabilization. These strong π-type interactions are indicative of enhanced aromaticity and conjugation, heavily influenced by halogen substitution patterns.

3.1.4.2 Lone Pair (n) → π and n → σ Interactions (Lactam–Enol Resonance)

Lone pairs on nitrogen and oxygen atoms contribute substantially to resonance stabilization and electron delocalization. The *n_2(N3) → π*(C5–C9)* interaction (Row 57) is particularly noteworthy, with a value of 98.28 kcal/mol in ISTA-10F, highlighting strong resonance interaction between nitrogen's lone pair and the extended aromatic π-system, influenced by halogen substitution. Similarly, interactions such as: *n_2(N3) → π*(C4–C5)* and *n_2(N3) → π*(O2–C7)* (Rows 55–56) show stabilization energies in the range of 80–87 kcal/mol, indicating significant charge delocalization from nitrogen into neighboring π* orbitals. Interestingly, the *n_2(N3) → π*(O2–C7)* interaction decreases from 87.38 kcal/mol (ISTA) to ~82 kcal/mol (ISTA-10F), suggesting that halogenation reduces lone-pair electron donation, likely due to inductive effects. In contrast, *n_2(O1) → σ*(C6–C7)* (Row 48) remains nearly unchanged across derivatives, indicating oxygen-based interactions are less sensitive to halogen substitution.

3.1.4.3 σ → σ and Hyperconjugative Interactions

Moderate hyperconjugative effects are observed via σ → σ* transitions: *σ(C6–C7) → σ*(C4–C8)* (Rows 11, 27) show values around 5.32–5.43 kcal/mol and *σ(N3–C7) → σ*(C5–C9)* (Row 9) shows 5.67–6.06 kcal/mol. These modest stabilization energies reflect hyperconjugative interactions slightly modulated by halogen substitution, with potential implications on bond strength and molecular conformation.

3.1.4.4 Halogen-Related Lone Pair Interactions (n(X) → π or n → n)

A notable characteristic of the halogen-substituted derivatives particularly ISTA-10A, ISTA-10B, and ISTA-10C, is the active participation of halogen lone pairs in conjugative resonance pathways. This is evidenced by significant donor–acceptor interactions such as *n_3*(Br14) → π*(C8–C10) with interaction energies ranging from 6.93 to 11.86 kcal/mol (Row

69), n_3(X15) → π*(C9–C11) ranging from 9.07 to 18.07 kcal/mol (Row 66), and n_3(Br14) → n_1(C10) contributing approximately 15 kcal/mol (Row 60). These interactions are absent in the unsubstituted ISTA, highlighting the unique electronic delocalization introduced by halogen substitution. These interactions confirm that halogen lone pairs actively participate in delocalization, enhancing molecular resonance and stability beyond mere inductive effects. ISTA-10C exhibits weaker halogen π donation (~9.07 kcal/mol), possibly due to the nature or position of the substituent.

3.1.5 Chemical Implications and Resonance Tuning via Halogenation

The introduction of halogen atoms significantly alters the electronic structure, resonance patterns, and stabilization pathways of the isatin anionic enol system. The highest interaction energy values, particularly for π → π* and n → π* transitions, emphasize the role of extended conjugation and lone pair delocalization in molecular stability. While σ → σ* interactions exist, they are secondary to the more dominant π-conjugative and lone-pair resonance effects. Notably, halogen lone pairs themselves contribute to resonance stabilization, highlighting the complexity and versatility of halogen-substituted systems. These findings have direct implications for the design of reactive or functional isatin derivatives. The observed electronic effects can influence reactivity (electrophilicity/nucleophilicity), spectroscopic shifts, and tautomeric preferences. Thus, understanding the resonance contributions and orbital interactions modulated by halogens is vital for both synthetic strategy and predictive computational modeling of heterocyclic systems.

3.2 TD-DFT Analysis and UV–Visible Spectral Features

Time-dependent DFT (TD-DFT) calculations were performed to analyze the electronic transitions and absorption characteristics of halogen-substituted isatin anions. The transitions were classified into three spectral groups *viz.* ES1, ES2, and ES3 (Table 3), based on their energy (wavelength) ranges and oscillator strengths (f).

Table 3 Calculated energy of transition (eV) corresponding to λ_{max} values (nm) and Oscillator strength

	ES1				ES2			
SPECIES	ORBITAL NO	ENERGY (eV)	λ (nm)	f	ORBITAL NO	ENERGY (eV)	λ (nm)	f
ISTA	38 to 39	2.2362	554.44	0.0180	37 to 39	2.3723	522.64	0.0000
ISTA-10	55 to 56	2.1624	573.35	0.0186	54 to 56	2.3295	532.23	0.0000
ISTA-10A	59 to 60	2.2779	544.30	0.0163	58 to 60	2.3882	519.14	0.0000
ISTA-10B	63 to 64	2.2096	561.11	0.0188	62 to 64	2.3308	531.93	0.0000
ISTA-10C	72 to 73	2.1969	564.37	0.0191	71 to 73	2.3211	534.16	0.0000
ISTA-10D	59 to 60	2.1553	575.25	0.0248	58 to 60	2.3204	534.32	0.0000
ISTA-10E	63 to 64	2.1538	575.66	0.0235	62 to 64	2.3176	534.97	0.0000
ISTA-10F	72 to 73	2.1530	575.86	0.0237	71 to 73	2.3154	535.49	0.0000

	ES3			
SPECIES	ORBITAL NO	ENERGY (eV)	λ (nm)	f
ISTA	35 to 39	3.8995	317.95	0.0002
ISTA-10	52 to 56	3.8667	320.65	0.0002
ISTA-10A	56 to 60	3.9471	314.11	0.0002
ISTA-10B	60 to 64	3.8784	319.68	0.0002
ISTA-10C	72 to 74	3.6541	339.31	0.0000
ISTA-10D	56 to 60	3.8999	317.92	0.0001
ISTA-10E	60 to 64	3.8795	319.59	0.0001
ISTA-10F	67 to 73 and 69 to 73	3.8676	320.57	0.0001

3.2.1 ES1 Transitions: Visible Region (Green–Yellow, ~544–576 nm)

The ES1 transitions occur predominantly in the green–yellow region of the visible spectrum, between 544 and 576 nm, corresponding to low-energy π → π* or n → π* transitions. These are the most intense and allowed transitions, exhibiting measurable oscillator strengths. Among all derivatives, ISTA-10D shows the highest oscillator strength (f = 0.0248), indicating

the strongest and most probable electronic transition in this group. Derivatives like ISTA-10E and ISTA-10F also exhibit relatively high oscillator strengths in this region, suggesting enhanced visible-region absorption.

These transitions represent the primary absorption bands for the anionic species and are expected to dominate their UV–Vis spectra. The enhanced oscillator strengths in halogenated derivatives imply that halogen substitution facilitates stronger orbital overlap and more allowed transitions, potentially making these compounds suitable for optical and chromophoric applications.

3.2.2 ES2 Transitions: Visible Region (Green, ~519–535 nm) – Forbidden Transitions

Such transitions may originate from n → π* excitations involving non-bonding orbitals with minimal spatial overlap, resulting in low transition dipole moments. Although present computationally, these ES2 transitions are unlikely to contribute significantly to experimental spectra.

3.2.3 ES3 Transitions: Ultraviolet Region (~314–339 nm) – Weak Transitions

Transitions in the ES3 group fall in the ultraviolet region (~314–339 nm), representing higher-energy excitations. These are mostly π → π* or n → π* transitions involving core or deeper molecular orbitals, typically observed as secondary or minor absorption bands. The oscillator strengths for ES3 transitions are very small (f ≈ 0.0001–0.0002), reflecting low-intensity, weakly allowed transitions. For example, ISTA-10C exhibits an extremely weak transition at 339.31 nm (f = 0.0000), effectively making it a forbidden or non-observable transition. Despite their weak nature, these transitions may still appear as minor shoulders or weak peaks in UV–Vis spectra and provide additional insights into the electronic structure and orbital energy gaps.

3.2.4 UV-Visible Spectral Shifts and Substitution Effects

The UV-Visible spectral analysis reveals that all the investigated anions of the enol form of isatin and its halogenated derivatives exhibit prominent absorption in the visible region, particularly within the 500–580 nm range (ES1 and ES2 transitions), indicating strong π→π* and n→π* electronic transitions. Notably, the λmax values (ES1) shift slightly toward longer wavelengths (bathochromic shift) in the halogenated derivatives (e.g., ISTA-10F: 575.86 nm, ISTA-10E: 575.66 nm) compared to the parent ISTA molecule (554.44 nm), suggesting enhanced conjugation and electron delocalization due to the electron-withdrawing effect of halogens as shown in Figure 3. This red shift implies that halogen substitution stabilizes the LUMO, thereby reducing the HOMO–LUMO energy gap. Conversely, the ES3 transitions occur at shorter wavelengths (314–339 nm), corresponding to higher energy excitations. Among these, ISTA-10C displays a slightly longer λmax (339.31 nm), reflecting subtle differences in orbital configurations and substitution patterns. These spectral shifts underscore the impact of halogen substitution on the electronic structure, enabling fine-tuning of optical properties, a feature that could be exploited in designing molecular systems for optoelectronic or sensing applications.

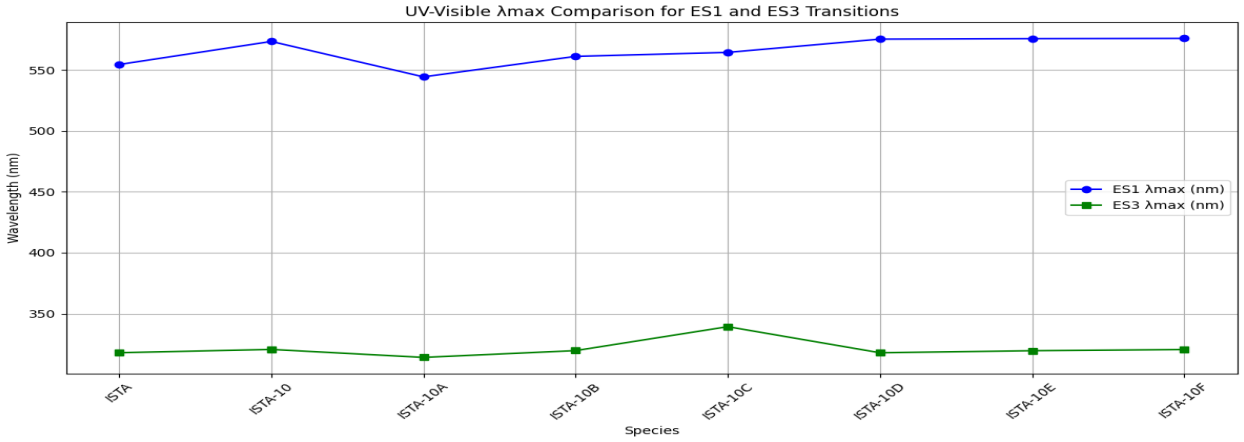

Figure 3 A graphical representation of UV-Visible λ_{max} for ISTA and its halogenated derivatives

3.2.5 Chemical and Optical Implications

The TD-DFT results across all species show that halogen substitution in the enol anion of isatin significantly modulates the electronic absorption characteristics. Notably, the λ_{max} values of the dominant ES1 transitions exhibit a clear bathochromic shift (red-shift) from 554.44 nm (ISTA) to ~575 nm in halogenated derivatives such as ISTA-10D, ISTA-10E, and ISTA-10F, suggesting an extension of π-conjugation and improved electron delocalization due to halogen involvement. This shift in absorption into the deeper visible region underscores the enhanced conjugation and electronic flexibility introduced by halogen atoms. The variation in oscillator strengths (f) for ES1–ES3 further highlights the electronic tunability of these systems. ES1 transitions are modestly allowed in all species (f ≈ 0.016–0.024), while ES2 transitions remain mostly forbidden (f = 0.0000), suggesting either symmetry-forbidden excitations or transitions with low overlap. ES3 transitions, which occur in the UV region (~314–340 nm), also show very weak oscillator strengths (f ≈ 0.0001–0.0002), indicating that these excitations likely correspond to secondary transitions influenced by subtle structural or electronic features of the π-system.

3.3 Correlation Between NBO Analysis and UV-Visible Spectra

The Natural Bond Orbital (NBO) analysis and UV-Visible spectral data reveal complementary insights into the electronic structure and conjugation patterns of isatin anion derivatives. A detailed correlation between the donor–acceptor interactions obtained from second-order perturbation theory (NBO) and the electronic transitions (ES1–ES3) computed using TD-DFT methods (B3LYP/6-311++G(d,p)) was carried out. The most significant π→π* delocalizations—particularly *π(C4–C5) → π*(C8–C10)* and *π(C4–C5) → π**(O1–C6) exhibit interaction energies ranging from 26.39 to 33.28 kcal/mol across various derivatives. These interactions contribute to the extended π-conjugation and lowering of the HOMO–LUMO energy gap, which is reflected in the bathochromic shift (red-shift) observed in the corresponding ES1 transitions in the UV-Visible region. For instance, ISTA, with a moderate π→π* delocalization energy (30.74 kcal/mol for π(C4–C5) → π*(C8–C10)), shows an ES1 absorption at 554.44 nm, while ISTA-10 with enhanced π-delocalization (33.28 kcal/mol) shows a red-shifted λ_max at 573.35 nm. This trend is consistent across other derivatives, such as ISTA-10D and ISTA-10F, where increased conjugative interactions (e.g., π*(O1–C6) → π*(O2–C7)) correspond to ES1 transitions above 575 nm. The oscillator strengths (f) for ES1 transitions, although low (~0.018–0.024), indicate weakly allowed π→π* transitions, in line with the frontier molecular orbital symmetry and electron distribution. These transitions primarily arise from HOMO to LUMO excitations, often involving lone-pair (n) or π orbitals from heteroatoms (N, O) and aromatic carbons. Moreover, ES3 transitions, which correspond to higher energy excitations (~3.8–3.9 eV, λ ~ 314–339 nm), involve deeper π orbitals (e.g., orbital 35 to 39 in ISTA) and show negligible oscillator strength (f ~ 0.0001–0.0002), confirming their forbidden or weakly allowed nature. These transitions further support the influence of conjugated systems and substituent effects in tuning the UV absorption profile. Thus, the NBO donor–acceptor interactions provide a molecular-level explanation for the red-shift and intensity modulation observed in the UV-Visible spectra, especially in ES1 and ES2 regions. This correlation underlines the effect of π-delocalization and intramolecular charge transfer on the optical properties of isatin-based enolate anions, with implications for their photophysical behavior and molecular design. The ES2 group includes transitions in the green region (~519–535 nm) but shows oscillator strengths close to zero (f ≈ 0.0000) across all derivatives. While these transitions are theoretically allowed, their near-zero oscillator strengths imply they are practically forbidden or involve poorly overlapping orbitals, leading to negligible absorption intensity. The optical characteristics align with the NBO analysis, which revealed enhanced π → π* and n → π* interactions due to halogen lone pair participation. The observed increase in orbital delocalization and overlap is consistent with both the red-shifted λmax and the modestly improved oscillator strengths, reinforcing the conclusion that halogenation not only alters the electron distribution but also optimizes the compound's potential in photoresponsive applications, dye chemistry, and nonlinear optical (NLO) materials.

IV. CONCLUSION

In this study, we have explored the electronic structure and excitation behavior of the anionic enol form of isatin and its halogenated derivatives through an integrated Natural Bond Orbital (NBO) analysis and UV-Visible spectroscopic approach using TD-DFT. The NBO results revealed strong donor–acceptor interactions, especially lone-pair to π* and π to π* transitions, which were significantly influenced by halogen substitution. These interactions directly affected the electron delocalization and intramolecular charge transfer, indicating enhanced conjugative stabilization in halogenated derivatives. The TD-DFT-derived UV-Visible spectra correlated well with the NBO findings, confirming that halogen substitution not only alters the electron density distribution but also shifts the absorption maxima, influencing photophysical properties. This direct correlation between NBO charge delocalization patterns and spectroscopic behavior presents a novel insight into how electronic interactions manifest in observable spectral transitions. The novelty of this work lies in establishing a unified theoretical framework that bridges ground-state orbital interactions with excited-state properties, particularly in anionic systems—a domain rarely addressed in isatin derivatives. Furthermore, this study provides a foundation for designing tailored isatin-based molecules with specific electronic or photophysical properties, making it relevant for material science, optoelectronics, and pharmaceutical development, where functionalized aromatic systems are key. This correlation-based approach offers a valuable predictive tool for future molecular design and reinforces the importance of detailed electronic structure analysis in understanding and engineering molecular behavior in real-world applications.

ACKNOWLEDGEMENT

Authors are thankful to Shyama Prasad Vidyalaya Lodi Estate and Amit Kumar, Department of Chemistry, University of Delhi for supporting this work

REFERENCES

[1] Pandeya, S. N.; Smitha, S.; Jyoti, M.; Sridhar, S. K. Biological Activities of Isatin and Its Derivatives. *Acta Pharm.* 2005, *55*, 27–46.

[2] da Silva, J. F. M.; Garden, S. J.; Pinto, A. C. The Chemistry of Isatins: A Review from 1975 to 1999. *J. Braz. Chem. Soc.* 2001, *12*, 273–324.

[3] Sridhar, S. K.; Saravanan, M.; Ramesh, A. Synthesis and Antibacterial Screening of Hydrazones, Schiff and Mannich Bases of Isatin Derivatives. *Eur. J. Med. Chem.* 2001, *36*, 615–625.

[4] Katritzky, A. R.; El-Gendy, B. E.; Draghici, B. Tautomerism in Heterocycles. *J. Chem. Soc., Perkin Trans. 2* 1990, 153–160.

[5] Politzer, P.; Murray, J. S. Halogen Bonding: An Electrostatically Driven Highly Directional Noncovalent Interaction. *Chem. Rev.* 2010, *110*, 443–458.

[6] Auffinger, P.; Hays, F. A.; Westhof, E.; Ho, P. S. Halogen Bonds in Biological Molecules. *Proc. Natl. Acad. Sci. U.S.A.* 2004, *101*, 16789–16794.

[7] Reed, A. E.; Weinhold, F. Natural Bond Orbital Analysis of Near-Hartree–Fock Water Dimer. *J. Chem. Phys.* 1983, *78*, 4066–4073.

[8] Weinhold, F.; Landis, C. R. *Valency and Bonding: A Natural Bond Orbital Donor–Acceptor Perspective*; Cambridge University Press: Cambridge, 2005.

[9] Silverstein, R. M.; Webster, F. X.; Kiemle, D. J. *Spectrometric Identification of Organic Compounds*, 7th ed.; Wiley: New York, 2005.

[10] Arora, E.; Gulia, S. Thermodynamic and Reactivity Parameters of Anions of Enol Form of Isatin and Its Halogenated Derivatives: A Theoretical Study. *Int. J. Innov. Res. Technol.* 2025, *12*(7), 4387–4397.

[11] Arora, E. Theoretical and Spectroscopic Investigation of Isatin Derivatives Using DFT. *J. Emerg. Technol. Innov. Res.* 2023, *10*(6), 748–756.

[12] Frisch, M. J.; Trucks, G. W.; Schlegel, H. B.; et al. *Gaussian 09, Revision D.01*; Gaussian, Inc.: Wallingford CT, 2013.

[13] Becke, A. D. Density-Functional Thermochemistry. III. The Role of Exact Exchange. *J. Chem. Phys.* 1993, *98*, 5648–5652.

[14] Lee, C.; Yang, W.; Parr, R. G. Development of the Colle–Salvetti Correlation-Energy Formula into a Functional of the Electron Density. *Phys. Rev. B* 1988, *37*, 785–789..

[15] Parr, R. G.; Yang, W. *Density-Functional Theory of Atoms and Molecules*; Oxford University Press: New York, 1989.

[16] Casida, M. E. Time-Dependent Density Functional Response Theory for Molecules. In *Recent Advances in Density Functional Methods*; Chong, D. P., Ed.; World Scientific: Singapore, 1995; pp 155–192.